ACS APPLIED MATERIALS & INTERFACES

Research Article

www.acsami.org

Fluorinated Polyimide Gate Dielectrics for the Advancing the Electrical Stability of Organic Field-Effect Transistors

Yonghwa Baek,[†,⊥] Sooman Lim,[‡,⊥] Eun Joo Yoo,[§] Lae Ho Kim,[†] Haekyoung Kim,[‡] Seung Woo Lee,*[,§] Se Hyun Kim,*[,∥] and Chan Eon Park*[,†]

[†]Polymer Research Institute, Department of Chemical Engineering, Pohang University of Science and Technology, Pohang 790-784, South Korea

[‡]School of Materials Science and Engineering, [§]School of Chemical Engineering, and [∥]Department of Nano, Medical and Polymer Materials, Yeungnam University, Gyeongsan 712-749, South Korea

Supporting Information

ABSTRACT: Organic field-effect transistors (OFETs) that operated with good electrical stability were prepared by synthesizing fluorinated polyimide (PI) gate dielectrics based on 6FDA–PDA–PDA PI and 6FDA–CF3Bz–PDA PI. 6FDA–PDA–PDA PI and 6FDA–CF3Bz–PDA PI contain 6 and 18 fluorine atoms per repeat unit, respectively. These fluorinated polymers provided smooth surface topographies and surface energies that decreased as the number of fluorine atoms in the polymer backbone increased. These properties led to a better crystalline morphology in the semiconductor film grown over their surfaces. The number of fluorine atoms in the PI backbone increased, the field-effect mobility improved, and the threshold voltage shifted toward positive values (from −0.38 to +2.21 V) in the OFETs with pentacene and triethylsilylethynyl anthradithiophene. In addition, the highly fluorinated polyimide dielectric showed negligible hysteresis and a notable gate bias stability under both a N_2 environment and ambient air.

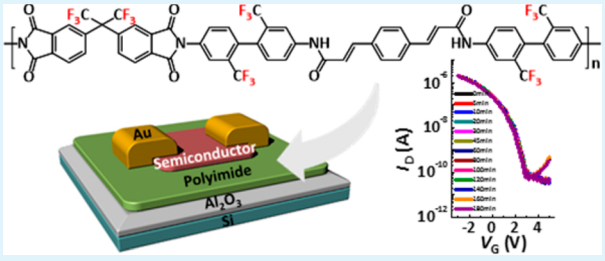

KEYWORDS: *organic field-effect transistor (OFET), gate dielectric, fluorinated polyimide, bias stress, charge trapping, operation stability*

1. INTRODUCTION

Over the past few decades, organic field-effect transistors (OFETs) have attracted considerable attention because they are cheap, easy to manufacture, and can be prepared through large-area solution process.[1−4] As a result of these advantages, OFETs are regarded as a leading device type in emerging electronic applications: flexible displays, sensors, low-cost portable memories, and radiofrequency identification (RFID) tags.[5−7]

One of the key factors that governs the electrical performances of OFETs involves tailoring the charge-trapping behavior properties at the interface between the semiconductor and the gate dielectric because most of charge carriers move through a few semiconductor monolayers formed near the dielectric surface.[8] Interface trap states typically arise from structural defects in the semiconductor film (e.g., grain boundaries), polar dielectric functional groups, and air molecules, such as H_2O and O_2. For this reason, a significant effort has been applied toward improving semiconductor/dielectric interfacial properties, including interface-engineering nanolayers through the introduction of hydrophobic self-assembled monolayers (SAMs) or ultrathin polymer films. These nanolayers can lead to the growth of a well-structured π-conjugated semiconductor molecules and can efficiently protect the channel from external trap-forming moieties.[9]

The processing and application aspects of OFETs require that the polymer material have good dielectric properties as well as being flexible, solution-processable, and adhesive toward a variety of organic layer materials.[10] Polymer dielectrics suitable for use in OFETs must also fulfill additional requirements: they should display good chemical resistance against solvents, heat, and plasma during layer deposition procedures. Pinhole-free dense film morphologies maintain a low leakage current in an OFET and prevent the adsorption of molecules from the air.[11] The development of polymer dielectric materials that provide favorable charge carrier transport and good bulk insulating properties remains a priority in this field of research.

This study reports the properties of several newly synthesized polyimides (PIs) having various numbers of fluorine atoms. The electrical performances of the OFETs prepared using these PIs as dielectrics are also described. PI offers excellent chemical and thermal stability; however,

Received: June 3, 2014
Accepted: August 5, 2014
Published: August 19, 2014

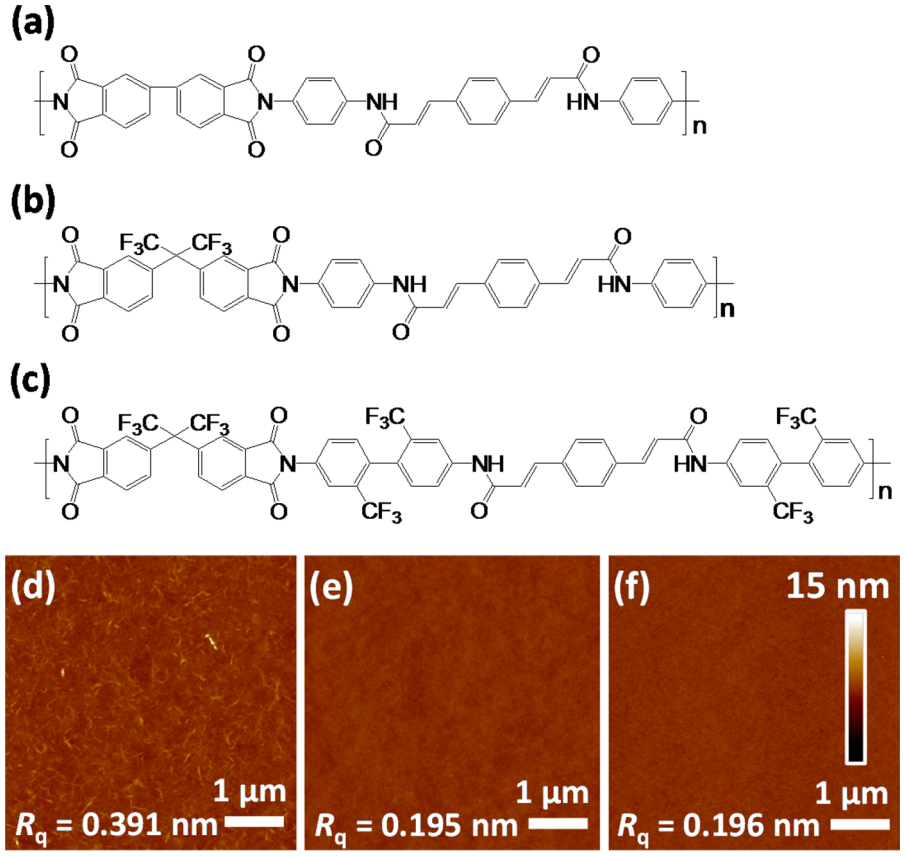

Figure 1. (a–c) Chemical structures of the PI dielectrics: (a) BPDA–PDA–PDA PI, (b) 6FDA–PDA–PDA PI, and (c) 6FDA–CF3Bz–PDA PI. (d–f) AFM images of the PI dielectrics in panels a, b, and c, respectively.

repeated imide groups create a very polar material and the use of PIs as dielectrics in an OFET can result in poor semiconductor growth or a large number of interface traps.[12] In general, the presence of fluorine atoms in a molecular assembly can improve the surface hydrophobicity and the chemical inertness of the surface. These properties stem from the properties of fluorine, which features a small atomic radius comparable to that of the hydrogen and the lowest polarizability of all atoms.[13] Fluorine-modified polymer dielectrics can impede trap creation, resulting in good electrical properties and reliable device operation.[14,15]

The fluorinated PI dielectrics were used to prepare low-operating-voltage OFETs bearing pentacene, triethylsilylethynyl anthradithiophene (TES-ADT), and PI/Al_2O_3 bilayer dielectrics. As the number of fluorine atoms in the PI backbone increased, the field-effect mobility (μ_{FET}) improved, and threshold voltage (V_{th}) shifted toward positive values (from −0.38 to +2.21 V). The highly fluorinated polyimide could realize electrically stable operation under both ambient air and a N_2 environment, with negligible hysteresis and a small shift in V_{th} (ΔV_{th}) under gate biasing.

2. EXPERIMENTAL SECTION

Materials. All materials, including triphenyl phosphite, pyridine, terephthalaldehyde, malonic acid, and potassium hydroxide, were purchased from Aldrich company and were used as received. 4,4′-(Hexafluoroisopropylidene)diphthalic anhydride (6FDA), 3,3′,4,4′-biphenyltetracarboxylic dianhydride (BPDA), and 2,2′-bis-(trifluoromethyl)benzidine were supplied by the Chriskev Company in Kansas, U.S.A. 6FDA was purified by recrystallization from acetic anhydride. The solvent used for the polymerization reaction, *N*-methyl-2-pyrrolidinone (NMP), was purchased from Aldrich, purified by distillation over calcium hydride, and stored over 4 Å molecular sieves.

Synthesis of 1,4-Phenylenediacrylic Acid (PDA). *p*-Phenylenediacrylic acid was prepared via a Knoevenagel condensation reaction from terephthalaldehyde and malonic acid.[16] Terephthalaldehyde (6.0 g, 44.7 mmol) and malonic acid (11.2 g, 107.4 mmol) were mixed in pyridine (25 mL), to which a few drops of piperidine were added. The solution was refluxed for 6 h, then cooled to room temperature and poured into a diluted KOH solution. After filtration, the filtrate was acidified with HCl (2 M) to form a white precipitate. The final product was filtered, washed with water, and dried in vacuo. The yield of the product was 7.32 g (75%); ^{1}H NMR (400 MHz, DMSO-d_6, TMS): d = 6.53–6.59 (d, −Ar−CH=C*H*−, 2H), 7.56–7.62 (d, −Ar−C*H*=CH−, 2H), 7.70 (s, Ar−*H*, 4H), 11.80–12.62 (s, −COO*H*, 2H)

Synthesis of Diamine Monomers. A novel diamine, 1,4-phenylenediacrylamide-*N*,*N*′-4,4′-bis(trifluoromethyl)benzidine (CF3Bz–PDA), was synthesized from a reaction of 2,2′-bis-(trifluoromethyl)benzidine and PDA using the following process. A mixture of PDA (5.0 g, 22.9 mmol), 2,2′-bis(trifluoromethyl)benzidine (36.7 g, 114.6 mmol), and triphenyl phosphite (14.2 g, 45.8 mmol) in NMP/pyridine (v/v = 4/1) was stirred at room temperature under nitrogen for 2 h.[17] The reaction mixture was heated to 120 °C for an additional 12 h and poured into methanol. The precipitated solids were separated by filtration and washed thoroughly with methanol. The crude product was purified by recrystallization from chloroform. The final product was filtered and dried in vacuo. The yield of the product was 13.8 g (73%); ^{1}H NMR (400 MHz, DMSO-d_6, TMS): d = 5.45–5.86 (s, −NH_2, 4H), 6.71–7.08 (m, −Ar−*H*, 4H), 7.24–7.32 (d, −Ar−C*H*=CH−CO−, 2H), 7.62–7.74 (d, −Ar−CH=C*H*−CO−, 2H), 7.74–7.82 (s, −Ar−*H*, 4H), 7.85–7.92 (d, −Ar−H, 2H), 8.20–8.29 (s, −Ar−*H*, 2H), 10.58–10.62 (s, −CO−N*H*−, 2H)

Table 1. Surface Properties and Capacitance of the PI Layers

gate dielectrics	water contact angle θ_{water} (deg)	diiodomethane contact angle θ_{dii} (deg)	surface energy [mJ/m^2]	capacitance [nF/cm^2]
BPDA−PDA−PDA PI	58	24	51.85	78.39
6FDA−PDA−PDA PI	70	35	44.32	78.11
6FDA−CF3Bz−PDA PI	76	40	40.81	76.77

In the same manner, 1,4-phenylenediacrylamide-*N*,*N*′-4,4′-dianiline (PDA−PDA) was synthesized using 1,4-phenylenediamine instead of 2,2′-bis(trifluoromethyl)benzidine. The yield of the product was 13.8 g (73%); ^{1}H NMR (400 MHz, DMSO-d_6, TMS): d = 4.51−5.08 (s, −N*H*$_2$, 4H), 6.54−6.57 (d, −Ar−*H*, 4H), 6.80−6.85 (d, −Ar−C*H*═CH−CO−, 2H), 7.34−7.37 (d, −Ar−CH═C*H*−CO−, 2H), 7.60−7.71 (s, −Ar−*H*, 4H), 9.63−9.78 (s, −CO−N*H*−, 2H)

Synthesis of Poly(amic acid). 6FDA−CF3Bz−PDA poly(amic acid) (PAA) was prepared by adding 1.0 equiv of 6FDA in a NMP solution and 1.0 equiv of CF3Bz−PDA, which were predissolved in NMP to form a 20.0 wt % solution, under nitrogen with vigorous stirring (see Figure 1). Once the addition was complete, the reaction flask was sealed tightly and the mixture was stirred for 48 h to allow polymerization. The mixture became homogeneous and viscous. In the same manner, BPDA−PDA−PDA and 6FDA−PDA−PDA PAA solutions were prepared from the reaction of PDA−PDA and BPDA and 6FDA, respectively. These solutions were filtered through a syringe-driven filter with a pore size of 1.0 μm and stored in a refrigerator until needed.

Materials and Preparation of the OFETs. A heavily n-doped Si substrate was cleaned with acetone for 30 min and dried. The Al_2O_3 (32 nm) dielectric layer was prepared by depositing it onto the substrate by atomic layer deposition (ALD). Three different PAA films were prepared by spin-casting onto the Al_2O_3/Si substrates at 3000 rpm using 8 wt % solutions. The 50 nm thick pentacene films were fabricated on the dielectrics via a vacuum process (deposition rate, 0.1−0.2 Å/s; vacuum pressure, − 10^{-6} Torr; substrate temperature, 25 °C). The as-spun PAA films were converted to PI films through stepwise thermal annealing under a N_2 atmosphere: 80 °C for 20 min, 150 °C for 30 min, 200 °C for 1 h, and 250 °C for 1 h. Finally, 30 nm thick PI films were deposited on the 32 nm thick Al_2O_3 gate dielectrics. Onto the PI/Al_2O_3 dielectrics were spin-cast TES-ADT films at 1000 rpm from a 1 wt % 1,2-dichloroethane (DCE) solution. Subsequent solvent annealing was carried out on the as-spun films under DCE vapor for ca. 30 min. A 100 nm thick gold electrode was deposited on the pentacene and TES-ADT semiconductor layers by thermal evaporation through a metal shadow mask. The channel lengths (L) and widths (W) of mask were 150 and 1500 μm, respectively.

Characterization. The transfer and output characteristics of the OFETs were measured using a Keithley 4200 SCS unit in a N_2-purged glovebox (the concentrations of H_2O and O_2 were maintained at less than 0.1 ppm) or under ambient air [25%, 55%, and 70% relative humidity (R.H.)]. Threshold voltage (V_{th}) was calculated from the transfer curve in the saturation regime swept over the gate voltage range V_G = +5 to −3 V. The surface energy (γ_s) of each PI film was calculated by measuring the contact angle using two test liquids (DI water and diiodomethane). The γ_s values were calculated according to the following equation by fitting to the measured values of the contact angles (Table 1):

$$1 + \cos\theta = \frac{2(\gamma_s^d)^{1/2}(\gamma_{lv}^d)^{1/2}}{\gamma_{lv}} + \frac{2(\gamma_s^p)^{1/2}(\gamma_{lv}^p)^{1/2}}{\gamma_{lv}}$$

where γ_{lv} is the surface energy of the liquid and the superscripts d and p refer to the dispersive and polar components, respectively. The surfaces of the PI and TES-ADT films were characterized by atomic force microscopy (AFM) in tapping mode (Bruker Nanoscope). Two-dimensional grazing-incidence X-ray diffraction (2D GIXD) experiments were performed at the 3C beamline (wavelength = 0.137 nm) at the Pohang Accelerator Laboratory (PAL). The incidence angle of the X-ray beam was set to 0.14° between the critical angles of the films and the substrate. The capacitance was characterized by fabricating a metal−insulator−metal (MIM) capacitor via the thermal deposition of gold onto the PI/Al_2O_3/heavily doped Si substrate. The measurements were performed using an Agilent 4284 precision LCR meter.

3. RESULTS AND DISCUSSION

Dielectric Properties of Fluorinated Polyimide Films. Figure 1 shows the chemical structures of the PI dielectrics tested in this experiment: (a) BPDA−PDA−PDA PI, (b) 6FDA−PDA−PDA PI, and (c) 6FDA−CF3Bz−PDA PI. 6FDA−PDA−PDA PI and 6FDA−CF3Bz−PDA PI samples, which had 6 or 18 fluorine atoms per repeat unit in the polymer chain, were examined for their utility as fluorinated polymer dielectric materials. For comparison the BPDA−PDA−PDA PI, which contained no fluorine atoms, was used as a reference. The AFM images shown in Figure 1d−f show that the BPDA−PDA−PDA PI surface was somewhat rougher with a relatively high root-mean-square (rms) roughness value of 0.391 nm compared with the other fluorinated samples, which exhibited amorphous smooth surface morphologies without prominent features. The rms values were 0.195 nm (6FDA−PDA−PDA PI) and 0.196 nm (6FDA−CF3Bz−PDA PI). The dielectric surface roughness effects (e.g., peak-to-peak height of the undulated surface) significantly influenced the dynamic behavior of the semiconductor film growth (nucleation and diffusion of molecules), reducing the extent of π-conjugation and introducing structural mismatch and defects into the semiconductor film.[18] Table 1 indicates the values of the water contact angles (θ_{water}) and surface energies for the three polyimide dielectrics. The θ_{water} value of BPDA−PDA−PDA PI was 58°, whereas the fluorinated PI films exhibited higher θ_{water} values (70° and 76° for 6FDA−PDA−PDA PI and 6FDA−CF3Bz−PDA PI, respectively.) In addition, the γ_s values for these polyimide dielectrics decreased from 51.85 (BPDA−PDA−PDA PI) to 40.81 mJ/m^2 (6FDA−CF3Bz−PDA PI) as the number of fluorine atoms in the polymer backbone increased. The values of γ_s included the sum of the polar and dispersion components, which were attributed to the interactions among permanent dipoles (including hydrogen bonds) and instantaneous dipole moments, respectively.[19] The γ_s values depended upon the chemical composition and packing density of the outmost surface functionalities. For example, nonpolar or weakly interactive surfaces generally yielded lower γ_s values. The values of γ_s for the fluorocarbon materials decreased in the order of CH_2 > CH_3 > CF_2 > CF_3.[20,21] The presence of a greater number of fluorine atoms and a higher degree of close packing at the surface reduced γ_s, as mentioned in the Introduction.[22] The value of γ_s can provide a direct indicator of the intermolecular forces, which play a critical role in the semiconductor film morphology and interface trap formation. The semiconductor growth modes on a flat substrate were determined through competition between the molecule−molecule or molecule−substrate interactions.[23] Polar surface causes the adsorption of air molecules onto a semiconductor/dielectric interface and broaden the tail states at the band edges, resulting in interface trap states.[24]

Semiconductor Having a Crystalline Morphology, Grown on the Fluorinated Surface. The growth of a semiconductor layer with a crystalline morphology on the fluorinated polyimide surfaces was investigated by characterizing the growth of vacuum-deposited pentacene or a solution-processed TES-ADT using AFM and 2D GIXD experiments. Parts a–c of Figure 2 show pentacene films grown on a

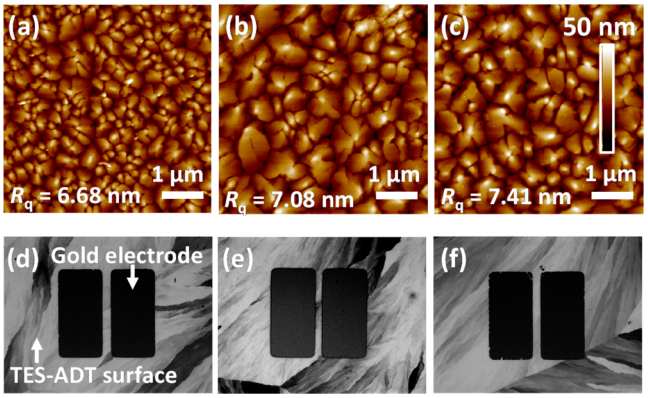

Figure 2. AFM images of 50 nm pentacene films and polarized optical microscopy images of TES-ADT on the PI dielectrics (a and d) BPDA–PDA–PDA PI, (b and e) 6FDA–PDA–PDA PI, and (c and f) 6FDA–CF3Bz–PDA PI, respectively. The channel lengths (L) and widths (W) in the mask were 150 and 1500 μm, respectively.

BPDA–PDA–PDA PI layer that exhibited a very small grain size of 400–450 nm. A relatively large grain size of 950–1000 nm and a layer-by-layer structure were observed in the fluorinated dielectrics including both 6FDA–PDA–PDA PI and 6FDA–CF3Bz–PDA PI. Generally, the grain size determines the diffusion of molecules adsorbed onto the surface.[25] A surface that favors longer traveling distances by a molecule prior to adsorption onto the surface (higher diffusion of the molecules) can reduce the number of nuclei that form on the surface, leading to larger complete grains.[26] A rough surface prevents surface diffusion of the molecules and increases the nucleation density. For this reason, the pentacene film prepared on the BPDA–PDA–PDA PI film formed small grains compared with the grains formed on other sample surfaces. The 2D GIXD analysis revealed a discernible crystalline morphology that depended on the properties of the substrate. Both 6FDA–PDA–PDA PI and 6FDA–CF3Bz–PDA PI mainly show thin-film phase pentacene crystal polymorphs, as determined by the (00l) reflections along the q_z axis (out-of-plane) and the $\{1, \pm1\}$ and $\{0, 2\}$ reflections along the q_{xy} axis (in-plane) (see Figure 3, parts b and c). On the other hand, the 2D GIXD patterns obtained from the BPDA–PDA–PDA PI sample displayed (00l)* reflections along the q_z direction and scattered peaks along the Debye ring (white asterisk). The in-plane reflections displayed highly scattered patterns along the Debye ring (peaks marked by arrows) These reflection peaks corresponded to a bulk phase pentacene crystal.[27] It is well-known that the coexistence of two different crystalline phases in a pentacene film can provide a barrier to charge carrier transport.[28]

Parts d–f of Figure 2 show polarized images of solution-processed TES-ADT films prepared on three different dielectric surfaces: BPDA–PDA–PDA PI, 6FDA–PDA–PDA PI, or 6FDA–CF3Bz–PDA PI. All films were fabricated by spin-casting, followed by solvent-assisted annealing, as described in

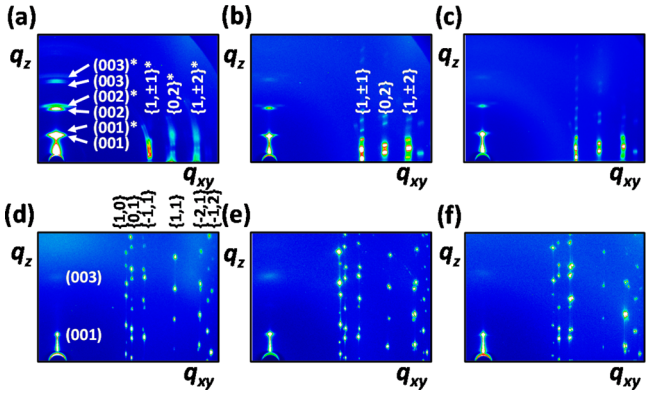

Figure 3. 2D GIXD patterns of the (a–c) pentacene and (d–f) TES-ADT on (a and d) BPDA–PDA–PDA PI, (b and e) 6FDA–PDA–PDA PI, and (c and f) 6FDA–CF3Bz–PDA PI.

the Experimental Section. Unlike the pentacene thin films, all samples exhibited crystals a few millimeters in size and a layer-by-layer structure with layer spacing of 16 Å, as characterized by AFM (Figure S1 in the Supporting Information). The 2D GIXD analyses confirmed that the TES-ADT films contained similar crystalline morphologies, regardless of the dielectric film on which they were grown. (see Figure 3d–f). The 2D GIXD patterns include intense (00l) and $\{hk\}$ plane reflections along the q_z (out-of-plane) and q_{xy} (in-plane) axes, respectively, corresponding to 3D multilayered triclinic structures.[29]

Electrical Performances of the OFETs Fabricated Using Fluorinated Dielectrics. Figure 4 shows the drain current–gate voltage (I_D–V_G) transfer characteristics of top-contact OFETs prepared using vacuum-deposited pentacene, solution-processed TES-ADT semiconductors, and PI/Al_2O_3 bilayer dielectrics including BPDA–PDA–PDA PI, 6FDA–PDA–PDA PI, or 6FDA–CF3Bz–PDA PI. The device structure is described in Figure 4a, and the device measurements were carried out in a N_2-purged glovebox (having water and oxygen concentrations of less than below 0.1 ppm). The pentacene films were used as deposited, whereas the TES-ADT films were completed by a solvent-assisted annealing step. The field-effect mobility (μ_{FET}) and threshold voltage (V_{th}) were calculated by fitting the experimental data to the following equation $I_D = (WC_i/2L)\mu_{FET}(V_G - V_{th})^2$, where C_i is the capacitance of the dielectric. All dielectrics investigated here exhibited similar C_i values (76.8–78.4 nF/cm^2). The turn-on voltage ($V_{turn\text{-}on}$), subthreshold slope (SS), and hysteresis were extracted from the I_D–V_G transfer curves on a logarithmic scale. The extracted electrical parameters of these OFETs are summarized in Table 2. Pentacene and TES-ADT OFETs operated stably within ±3 V, over the range +5 to −3 V, maintaining a transfer characteristics on/off ratio of -10^5. Figure 4d–f indicates that the TES-ADT-based OFETs displayed typical p-type characteristics with a clear transition in the output characteristics from linear to saturation behavior. The μ_{FET} values of the fluorinated polyimide-based OFETs were higher than those of the PI-based OFETs prepared with both the pentacene and the TES-ADT semiconductors, reaching values as high as 0.23 cm^2/(V s) for the TES-ADT OFETs containing 6FDA–CF3Bz–PDA PI (see Table 2). As discussed previously, the polar imide groups on the PI acted as charge carrier traps in the channel and decreased μ_{FET}. The poor pentacene growth on the BPDA–PDA–PDA PI also significantly influenced charge carrier transport. 6FDA–PDA–

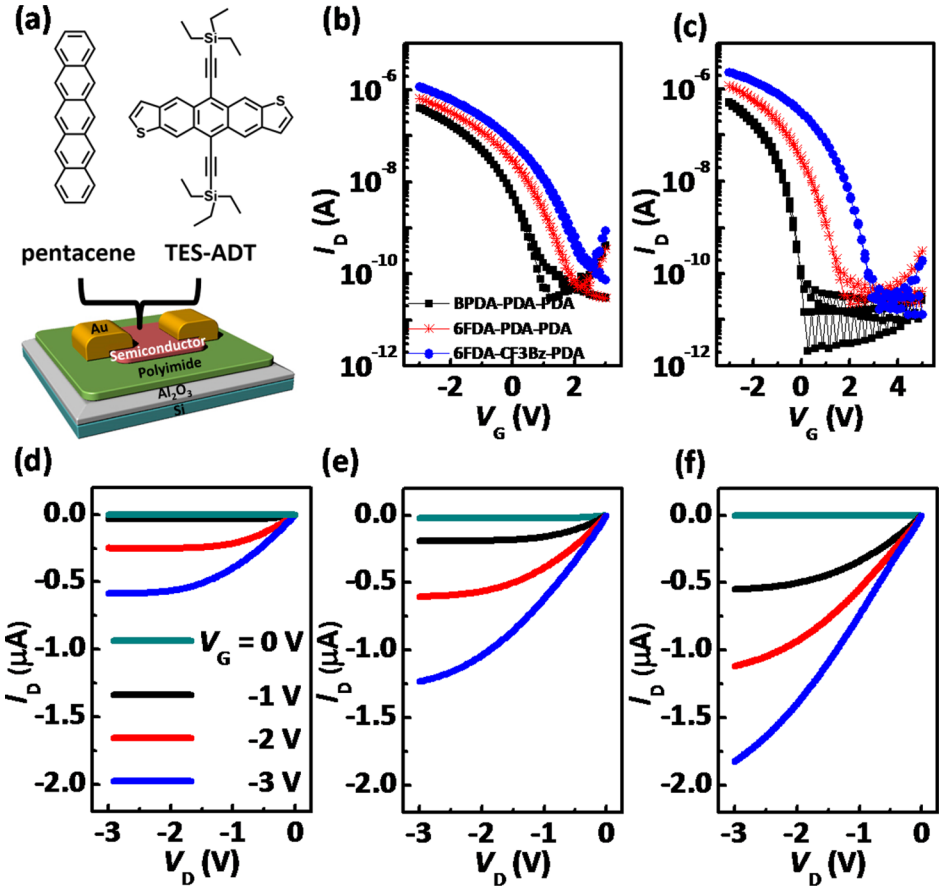

Figure 4. (a) Schematic diagram of the top-contact OFETs investigated in this study. (b and c) Drain current−gate voltage (I_D−V_G) transfer characteristics of (b) pentacene and (c) TES-ADT based OFETs containing BPDA−PDA−PDA PI, 6FDA−PDA−PDA PI, and 6FDA−CF3Bz−PDA PI before and after an applied gate bias stress of V_G = −3 V (V_D = 0) for 3 h in N_2. (d−f) Output characteristics of the TES-ADT-based OFETs containing BPDA−PDA−PDA PI, 6FDA−PDA−PDA PI, and 6FDA−CF3Bz−PDA PI, respectively.

Table 2. OFET Performances of Pentacene and TES-ADT-Based PI Dielectrics under a N_2 Environment

semiconductors	gate dielectrics	mobility [cm^2/(V s)]	V_{th} [V]	ΔV_{th} [V]	on/off ratio	SS [V per decade]
pentacene	BPDA−PDA−PDA PI	0.12	−0.05		1.34×10^4	0.56
	6FDA−PDA−PDA PI	0.15	0.36		1.27×10^4	0.60
	6FDA−CF3Bz−PDA PI	0.23	0.64		7.23×10^3	0.77
TES-ADT	BPDA−PDA−PDA PI	0.20	−0.38	−2.11	6.40×10^4	0.18
	6FDA−PDA−PDA PI	0.21	0.74	−2.12	4.24×10^4	0.43
	6FDA−CF3Bz−PDA PI	0.23	2.21	−0.50	1.04×10^5	0.33

PDA PI and 6FDA−CF3Bz−PDA PI OFETs exhibited more positive values of $V_{turn\text{-}on}$ and V_{th} than the BPDA−PDA−PDA PI in both the pentacene and TES-ADT samples (Figure 4, parts b and c). Although the fluorinated surface possessed a lower surface energy than the surfaces that lacked fluorine atoms, the C−F bonds provided a relatively high dipole moment due to the high electronegativity of the fluorine atoms. Early studies of the dielectric surface chemistry have demonstrated that surfaces with a strong electron affinity and/or acidic character should preferentially attract electrons to the semiconductor side, thereby increasing the hole injection for charge balancing and shifting $V_{turn\text{-}on}$ and V_{th} toward positive values.[30]

Gate Bias Stability of the OFETs Fabricated with Fluorinated Dielectrics. Further physical insight into interface trap formation in the presence (or absence) of fluorine atoms in the polyimide dielectrics was sought by investigating the electrical stabilities of the corresponding OFETs and performing gate bias stress experiments on the TES-ADT-based OFETs. Our TES-ADT films displayed similar crystalline morphologies when grown on each of the three dielectrics, as mentioned above (Figures 2 and 3). Moreover, device measurements were carried out in a N_2-purged glovebox to rule out degradation of the semiconductor due to compounds in the air. These experiments were designed to focus exclusively on the relationship between the gate bias stability and the interface traps. All devices tested here were operated over the range +5 to −3 V and were found to display clear p-type characteristics. Figure 5 shows the transfer curves of the TES-ADT OFETs prepared with BPDA−PDA−PDA PI, 6FDA−PDA−PDA PI, and 6FDA−CF3Bz−PDA PI dielectrics, as a function of the bias stress time. A sustained V_G of −3 V was applied to the devices over 3 h, and V_D was held constant at 0 V (the source electrode was grounded during device operation). The resulting shifts in V_{th} from the initial state (ΔV_{th}) after applying a gate bias stress were −2.11 V (BPDA−PDA−PDA

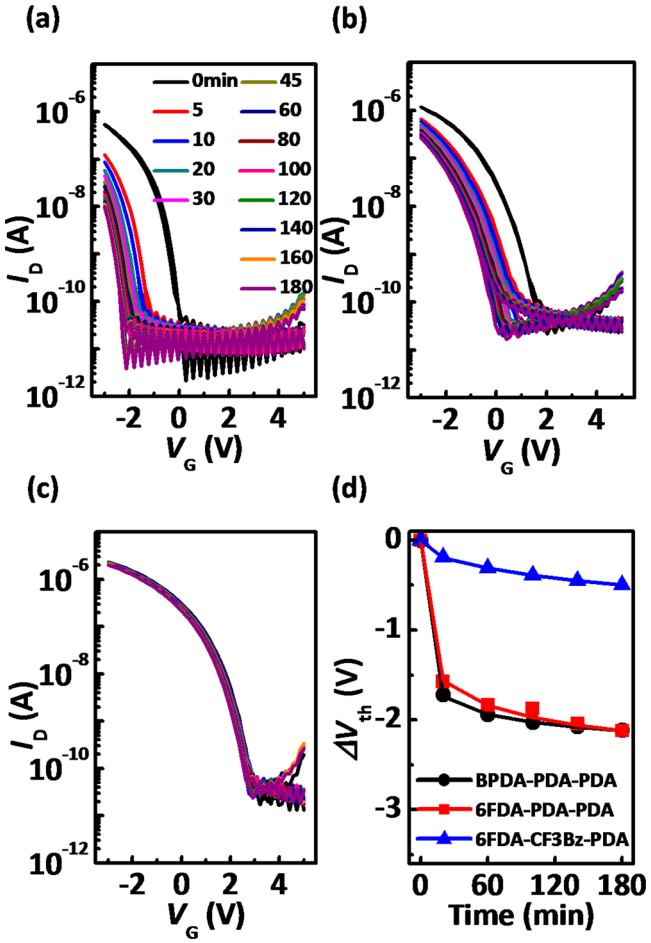

Figure 5. Drain current−gate voltage (I_D−V_G) transfer characteristics of TES-ADT-based OFETs containing (a) BPDA−PDA−PDA PI, (b) 6FDA−PDA−PDA PI, and (c) 6FDA−CF3Bz−PDA PI before and after an applied gate bias stress of V_G = −3 V (V_D = 0) for 3 h and (d) threshold voltage shifts (ΔV_{th}) of the TES-ADT-based OFETs as a function of the bias stress time under a N_2 environment.

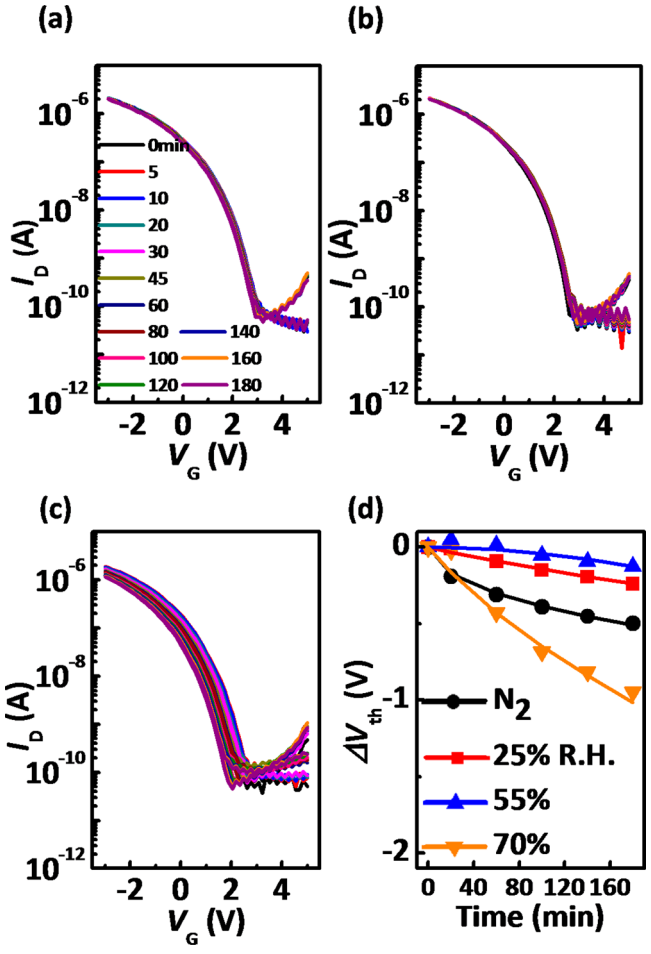

Figure 6. Drain current−gate voltage (I_D−V_G) transfer characteristics of TES-ADT-based OFETs prepared with 6FDA−CF3Bz−PDA PI before and after an applied gate bias stress of V_G = −3 V (V_D = 0) for 3 h in (a) 25% R.H., (b) 55% R.H., and (c) 70% R.H. and (d) threshold voltage shifts (ΔV_{th}) of the TES-ADT-based OFETs as a function of the bias stress time various humidity conditions.

PI), −2.12 V (6FDA−PDA−PDA PI), and −0.50 V (6FDA−CF3Bz−PDA PI). The magnitude of ΔV_{th} was inversely proportional to the number of fluorine atoms present in the polyimide backbone, suggesting that the fluorine group effectively prevented the creation of interface traps under the gate bias stress. The 6FDA−CF3Bz−PDA PI OFETs exhibited the most negligible hysteresis, defined as the difference between the off-to-on and on-to-off transfer curves. In general, the gate bias stressed ΔV_{th} values and the hysteresis resulted from relatively long lifetime or energetically deep traps that could immobilize charges in the channel by capturing free carriers, leading to a decrease in the current and/or ΔV_{th}.[31] The traps that contributed device instability behaviors could be distinguished based on their lifetimes, reported as 10 s to 1 min (hysteresis) or of the order of hours (bias stressed ΔV_{th}).[32]

The device instabilities in the TES-ADT OFETs prepared using 6FDA−CF3Bz−PDA PI under ambient air were characterized by conducting device measurements under various humidity conditions (25%, 55%, and 70% R.H.). It should be noted that adsorbed water molecules and polar surface groups induced charge traps that degraded the OFET performances.[33] As shown in Figure 6, the 6FDA−CF3Bz−PDA PI devices exhibited negligible hysteresis at all values of R.H. tested here. By contrast, the gate bias induced ΔV_{th} values at 25% and 55% R.H. were −0.24 and −0.13 V, respectively, comparable to those of OFETs measured under a N_2 atmosphere. In particular, at 70% R.H., the device produced a ΔV_{th} of −0.95 V after gate bias stressing, although this value was lower than the values obtained from the BPDA−PDA−PDA PI (−2.11 V) and 6FDA−PDA−PDA PI (−2.12 V) samples characterized under a N_2 environment. The 6FDA−CF3Bz−PDA PI surface inhibited trap creation related to the bias-stressed ΔV_{th} by preventing the adsorption of water molecules at a relatively low R.H., less than 55%. Above this value, water-induced traps began to form at the interface. The incorporation of additional fluorine atoms at the surface is expected to provide a more stable operation.

The dependence of the OFET ΔV_{th} on the number of fluorine atoms present in the polyimide or R.H. could be modeled using a stretched exponential equation

$$\frac{V_{th} - V_{th,i}}{V_G - V_{th,i}} = 1 - \frac{1}{\{1 + \exp[(E_{th} - E_A)/k_B T_0]\}^{1/(\alpha-1)}}$$

where $V_{th,i}$, E_A, $k_B T_0$, and α denote the initial V_{th}, typical activation energy for trap creation, slope of the distribution in the E_A, and a constant, respectively. E_{th}, the thermalization energy, is defined by $k_B T \ln(\nu t)$. Here, k_B and ν are the

dx.doi.org/10.1021/am5035076 | ACS Appl. Mater. Interfaces 2014, 6, 15209−15216

Table 3. E_A and k_BT_0 Values of the TES-ADT-Based OFETs Prepared Using PIs Dielectrics under a N_2 Environment

gate dielectrics	BPDA−PDA−PDA PI	6FDA−PDA−PDA PI	6FDA−CF3Bz−PDA PI
E_A (eV)	0.510	0.606	0.702
k_BT_0 (eV)	0.100	0.110	0.057

Boltzmann constant and attempt-to-escape frequency, respectively. The fit was optimized by selecting the fitting parameters ν and α to be 10^5 Hz and 1.5, respectively, as determined for the TES-ADT sample in a previous study.[34] The curves of the ΔV_{th} values obtained at various stress times were clearly fit by this equation, as shown in Figures 5d and 6d. E_A and k_BT_0 increased as the number of fluorine atom increased or as the R.H. decreased. The values obtained from all devices are summarized in Tables 3 and 4. The E_A values of the BPDA−PDA−PDA PI, 6FDA−PDA−PDA PI, and 6FDA−CF3Bz−PDA PI samples were 0.510, 0.606, and 0.702 eV under a N_2 environment, respectively. The 6FDA−CF3Bz−PDA PI OFET yielded E_A values of 0.641 eV (25% R.H.), 0.592 eV (55% R.H.), and 0.590 eV (70% R.H.). These results suggested that the interface established by the TES-ADT and fluorinated polyimide interface suppressed trap creation toward the goal of realizing device reliability under both inert N_2 and ambient air.

Table 4. E_A and k_BT_0 Values of the TES-ADT-Based OFETs Prepared Using 6FDA−CF3Bz−PDA PI Dielectrics under Various Humidity Conditions

environment (6FDA−CF3Bz−PDA PI)	25% R.H.	55% R.H.	70% R.H.
E_A (eV)	0.641	0.592	0.590
k_BT_0 (eV)	0.029	0.013	0.029

4. CONCLUSION

In summary, we synthesized new fluorinated polyimides (PIs) for use the dielectrics in OFETs based on vacuum-deposited pentacene and solution-processed TES-ADT semiconductor layers. The introduction of fluorine atoms into the PI backbones tailored the surface properties of the PI dielectrics, such as the surface energy and roughness. On the fluorinated PI dielectrics, the vacuum-deposited pentacene films showed better crystalline morphologies (thin-film phase crystals and large 950−1000 nm grain sizes) compared to the morphologies prepared on the nonfluorinated surface (which displayed coexistent thin films and bulk phase crystals with 400−450 nm grain sizes). In addition, millimeter-sized TES-ADT crystals developed by solution processing (spin-casting and solvent annealing). The pentacene and TES-ADT OFETs prepared on the 6FDA−CF3Bz−PDA PI dielectrics yielded μ_{FET} values of 0.23 $cm^2/(V\ s)$.

In particular, the electrical stabilities of the OFETs were demonstrated through gate bias stress experiments conducted on samples prepared with varying numbers of fluorine atoms in the dielectric polymer. An increase in the number of fluorine atoms in the PI backbone yielded a higher electrical stability in the TES-ADT OFETs (a smaller ΔV_{th} under the applied gate bias), as well as more negligible hysteresis. The TES-ADT OFETs prepared using highly fluorinated PI (6FDA−CF3Bz−PDA PI) showed good device operation under humid conditions (− 55% R.H.), comparable to the performances obtained under an inert N_2 atmosphere. This study revealed that OFETs containing fluorine groups in the gate dielectrics operated stably under a variety of conditions because they prevented the creation of semiconductor/dielectric interface traps.

■ ASSOCIATED CONTENT

Supporting Information

AFM image of TES-ADT films on the 6FDA−CF3Bz−PDA PI. This material is available free of charge via the Internet at http://pubs.acs.org.

■ AUTHOR INFORMATION

Corresponding Authors

*E-mail: leesw1212@ynu.ac.kr. Fax: +82-53-810-4631. Phone: +82-53-810-2516.

*E-mail: shkim97@yu.ac.kr. Fax: +82-53-810-4686. Phone: +82-53-810-2779.

*E-mail: cep@postech.ac.kr. Fax: +82-54-279-8298. Phone: +82-54-279-2269.

Author Contributions

⊥Y.B. and S.L. contributed equally to this work.

Notes

The authors declare no competing financial interest.

■ ACKNOWLEDGMENTS

This work was also supported by a Grant from the National Research Foundation of Korea (NRF), funded by the Korean Government (MSIP) (2014R1A2A1A05004993 and 2014R1A1A1005896).

■ REFERENCES

(1) Facchetti, A. Organic Semiconductors: Made to Order. *Nat. Mater.* **2013**, *12*, 598−600.

(2) Yi, H. T.; Payne, M. M.; Anthony, J. E.; Podzorov, V. Ultra-flexible Solution-processed Organic Field-effect Transistors. *Nat. Commun.* **2012**, *3*, 1259.

(3) Fukuda, K.; Hikichi, K.; Sekine, T.; Takeda, Y.; Minamiki, T.; Kumaki, D.; Tokito, S. Strain Sensitivity and Durability in P-type and N-type Organic Thin-film Transistors with Printed Silver Electrodes. *Sci. Rep.* **2013**, *3*, 2048.

(4) Park, Y. M.; Jimison, L. H.; Desai, A.; Salleo, A. Solution-Processable Zirconium Oxide Gate Dielectrics for Flexible Organic Field Effect Transistors Operated at Low Voltages. *Chem. Mater.* **2013**, *25*, 2571−2579.

(5) Yokota, T.; Kuribara, K.; Tokuhara, T.; Zschieschang, U.; Klauk, H.; Takimiya, K.; Sadamitsu, Y.; Hamada, M.; Sekitani, T.; Someya, T. Flexible Low-Voltage Organic Transistors with High Thermal Stability at 250° C. *Adv. Mater.* **2013**, *25*, 3639−3644.

(6) Khan, H. U.; Roberts, M. E.; Knoll, W.; Bao, Z. Pentacene Based Organic Thin Film Transistors as the Transducer for Biochemical Sensing in Aqueous Media. *Chem. Mater.* **2011**, *23*, 1946−1953.

(7) Baeg, K. J.; Khim, D.; Kim, J.; Yang, B. D.; Kang, M.; Jung, S. W.; You, I. K.; Kim, D. Y.; Noh, Y. Y. High-Performance Top-Gated Organic Field-Effect Transistor Memory using Electrets for Monolithic Printed Flexible NAND Flash Memory. *Adv. Funct. Mater.* **2012**, *22*, 2915−2926.

(8) Dinelli, F.; Murgia, M.; Levy, P.; Cavallini, M.; Biscarini, F.; de Leeuw, D. M. Spatially Correlated Charge Transport in Organic Thin Film Transistors. *Phys. Rev. Lett.* **2004**, *92*, 116802.

(9) McDowell, M.; Hill, I.; McDermott, J.; Bernasek, S.; Schwartz, J. Improved Organic Thin-Film Transistor Performance Using Novel

Self-Assembled Monolayers. *Appl. Phys. Lett.* **2006**, *88*, 073505−073505−3.
(10) Choi, M.-C.; Kim, Y.; Ha, C.-S. Polymers for Flexible Displays: From Material Selection to Device Applications. *Prog. Polym. Sci.* **2008**, *33*, 581−630.
(11) Facchetti, A.; Yoon, M. H.; Marks, T. J. Gate Dielectrics for Organic Field-Effect Transistors: New Opportunities for Organic Electronics. *Adv. Mater.* **2005**, *17*, 1705−1725.
(12) Lee, S.; Koo, B.; Shin, J.; Lee, E.; Park, H.; Kim, H. Effects of Hydroxyl Groups in Polymeric Dielectrics on Organic Transistor Performance. *Appl. Phys. Lett.* **2006**, *88*, 162109−162109−3.
(13) Zhao, X. Y.; Liu, H. J. Review of Polymer Materials with Low Dielectric Constant. *Polym. Int.* **2010**, *59*, 597−606.
(14) Kalb, W. L.; Mathis, T.; Haas, S.; Stassen, A. F.; Batlogg, B. Organic Small Molecule Field-Effect Transistors with Cytop Gate Dielectric: Eliminating Gate Bias Stress Effects. *Appl. Phys. Lett.* **2007**, *90*, 092104−092104−3.
(15) Walser, M.; Kalb, W.; Mathis, T.; Batlogg, B. Low-Voltage Organic Transistors and Inverters with Ultrathin Fluoropolymer Gate Dielectric. *Appl. Phys. Lett.* **2009**, *95*, 233301−233301−3.
(16) Zhao, J. S.; Wang, J. H.; He, W. B.; Ruan, Y. B.; Jiang, Y. B. Isolable Chiral Aggregates of Achiral π-Conjugated Carboxylic Acids. *Chem.—Eur. J.* **2012**, *18*, 3631−3636.
(17) Choi, K. H.; Lee, K. H.; Jung, J. C. Synthesis of New Poly (amide imide) s with (n-alkyloxy)phenyloxy Side Branches. *J. Polym. Sci., Part A: Polym. Chem.* **2001**, *39*, 3818−3825.
(18) Steudel, S.; De Vusser, S.; De Jonge, S.; Janssen, D.; Verlaak, S.; Genoe, J.; Heremans, P. Influence of the Dielectric Roughness on the Performance of Pentacene Transistors. *Appl. Phys. Lett.* **2004**, *85*, 4400−4402.
(19) Kim, J.; Friend, R.; Cacialli, F. Surface Energy and Polarity of Treated Indium−Tin−Oxide Anodes for Polymer Light-Emitting Diodes Studied by Contact-Angle Measurements. *J. Appl. Phys.* **1999**, *86*, 2774−2778.
(20) Graham, P.; Stone, M.; Thorpe, A.; Nevell, T. G.; Tsibouklis, J. Fluoropolymers with Very Low Surface Energy Characteristics. *J. Fluorine Chem.* **2000**, *104*, 29−36.
(21) Nishino, T.; Meguro, M.; Nakamae, K.; Matsushita, M.; Ueda, Y. The Lowest Surface Free Energy Based on-CF3 Alignment. *Langmuir* **1999**, *15*, 4321−4323.
(22) Song, X.; Zhai, J.; Wang, Y.; Jiang, L. Fabrication of Superhydrophobic Surfaces by Self-Assembly and Their Water-Adhesion Properties. *J. Phys. Chem. B* **2005**, *109*, 4048−4052.
(23) Yang, S. Y.; Shin, K.; Park, C. E. The Effect of Gate-Dielectric Surface Energy on Pentacene Morphology and Organic Field-Effect Transistor Characteristics. *Adv. Funct. Mater.* **2005**, *15*, 1806−1814.
(24) Kalb, W. L.; Haas, S.; Krellner, C.; Mathis, T.; Batlogg, B. Trap Density of States in Small-Molecule Organic Semiconductors: A Quantitative Comparison of Thin-Film Transistors with Single Crystals. *Phys. Rev. B* **2010**, *81*, 155315.
(25) Ruiz, R.; Choudhary, D.; Nickel, B.; Toccoli, T.; Chang, K.-C.; Mayer, A. C.; Clancy, P.; Blakely, J. M.; Headrick, R. L.; Iannotta, S. Pentacene Thin Film Growth. *Chem. Mater.* **2004**, *16*, 4497−4508.
(26) Zu Heringdorf, F.-J. M.; Reuter, M.; Tromp, R. Growth Dynamics of Pentacene Thin Films. *Nature* **2001**, *412*, 517−520.
(27) Kim, D. H.; Lee, H. S.; Yang, H.; Yang, L.; Cho, K. Tunable Crystal Nanostructures of Pentacene Thin Films on Gate Dielectrics Possessing Surface-Order Control. *Adv. Funct. Mater.* **2008**, *18*, 1363−1370.
(28) Matsubara, R.; Ohashi, N.; Sakai, M.; Kudo, K.; Nakamura, M. Analysis of Barrier Height at Crystalline Domain Boundary and In-Domain Mobility in Pentacene Polycrystalline Films on SiO2. *Appl. Phys. Lett.* **2008**, *92*, 242108−242108−3.
(29) Kim, S. H.; Jang, M.; Yang, H.; Anthony, J. E.; Park, C. E. Physicochemically Stable Polymer-Coupled Oxide Dielectrics for Multipurpose Organic Electronic Applications. *Adv. Funct. Mater.* **2011**, *21*, 2198−2207.
(30) Pernstich, K.; Haas, S.; Oberhoff, D.; Goldmann, C.; Gundlach, D.; Batlogg, B.; Rashid, A.; Schitter, G. Threshold Voltage Shift in Organic Field Effect Transistors by Dipole Monolayers on the Gate Insulator. *J. Appl. Phys.* **2004**, *96*, 6431−6438.
(31) Wang, S.; Minari, T.; Miyadera, T.; Aoyagi, Y.; Tsukagoshi, K. Bias Stress Instability in Pentacene Thin Film Transistors: Contact Resistance Change and Channel Threshold Voltage Shift. *Appl. Phys. Lett.* **2008**, *92*, 063305−063305−3.
(32) Goldmann, C.; Krellner, C.; Pernstich, K.; Haas, S.; Gundlach, D.; Batlogg, B. Determination of the Interface Trap Density of Rubrene Single-Crystal Field-Effect Transistors and Comparison to the Bulk Trap Density. *J. Appl. Phys.* **2006**, *99*, 034507.
(33) Wang, C.; Lee, W.-Y.; Nakajima, R.; Mei, J.; Kim, D. H.; Bao, Z. Thiol−ene Cross-Linked Polymer Gate Dielectrics for Low-Voltage Organic Thin-Film Transistors. *Chem. Mater.* **2013**, *25*, 4806−4812.
(34) Suemori, K.; Uemura, S.; Yoshida, M.; Hoshino, S.; Takada, N.; Kodzasa, T.; Kamata, T. Threshold Voltage Stability of Organic Field-Effect Transistors for Various Chemical Species in the Insulator Surface. *Appl. Phys. Lett.* **2007**, *91*, 192112−192112−3.